MDPI

Article

Orientation Control System: Enhancing Aerial Maneuvers for Quadruped Robots

Francesco Roscia [1], Andrea Cumerlotti [1,2], Andrea Del Prete [2], Claudio Semini [1] and Michele Focchi[1,3,*]

[1] Dynamic Legged Systems (DLS) lab, Istituto Italiano di Tecnologia (IIT), Genoa, Italy
[2] Industrial Engineering Department (DII), University of Trento, Trento, Italy
[3] Department of Information Engineering and Computer Science (DISI), University of Trento, Trento, Italy
* Correspondence: michele.focchi@unitn.it

Abstract: For legged robots, aerial motions are the only option to overpass obstacles that cannot be circumvent with standard locomotion gaits. In these cases, the robot must perform a leap to either jump onto the obstacle or fly over it. However, these movements represent a challenge because during the flight phase the Center of Mass (CoM) cannot be controlled, and the robot orientation has limited controllability. This paper focuses on the latter issue and proposes an Orientation Control System (OCS) consisting of two rotating and actuated masses (flywheels or reaction wheels) to gain control authority on the robot orientation. Because of the conservation of angular momentum, their rotational velocity can be adjusted to steer the robot orientation even when there are no contacts with the ground. The axes of rotation of the flywheels are designed to be incident, leading to a compact orientation control system that is capable of controlling both roll and pitch angles, considering the different moment of inertia in the two directions. We tested the concept with simulations on the robot Solo12.

Keywords: Legged robot, Orientation Control, Articulated Multi-body System

Citation: Roscia, F.; Cumerlotti, A.; Del Prete, A., Semini, C.; Focchi, M. Orientation Control System: Enhancing Aerial Maneuvers for Quadruped Robots. *Sensors* **2022**, *1*, 0. https://doi.org/

Received:
Accepted:
Published:

Publisher's Note: MDPI stays neutral with regard to jurisdictional claims in published maps and institutional affiliations.

1. Introduction

Legged robots are designed for traversing rough terrain. Different types of gaits, such as trot or crawl, have been developed for quadrupedal robots. Thanks to the progress of the last two decades, robots have become lighter and stronger, which has enabled them to perform agile locomotion. However, sometimes it is not possible to get around or over an obstacle with the gaits mentioned above, and jumps are required.

When the robot is in the air, the CoM moves on the ballistic trajectory, that is completely defined by the lift-off position and velocity. On the other hand, the base orientation can be changed exploiting the conservation of the system angular momentum. This means that it is possible to control the base angular velocity by changing the inertia of the robot, e.g., changing the joints configuration.

Nevertheless, the majority of quadrupeds are designed with light legs, resulting in limbs that have small influence on the total angular momentum.

Quadrupedal animals, like cats, can rearrange tail and trunk to correct the orientation during a fall [1]. Many works in the field of robotics used an additional link as a tail, like in [2] and [3]. This link rotates around an axis that does not pass through the robot CoM: the distances between the axis of rotation and the CoM of both trunk and tail result in a large effect on the total inertia even with a small tail mass. However, the placement of the additional link makes the resulting robot asymmetric. Moreover, due to its limited range of motion, a tail can be used only for a single jump, not for a repeated sequence [4]. It is possible to obtain a similar result by creating repetitive circular motions with the feet, like in [5] and [**?**]. In the latter work, the authors proposed special heavy boots for Mini Cheetah and used a neural network to calculate online joint trajectories. However, this solution unnecessarily increases the inertia of the legs, complicating the locomotion

Figure 1. The proposed Orientation Control System for for the 2.5 kg quadruped robot Solo12 consists of two 0.1 kg flywheels with incident rotation axes. Each wheel is located in a 3D-printed shell and mounted on the trunk body.

problem, which can no longer rely on the massless leg assumption. Another option is to use a Control Moment Gyroscope (CMG). It consists of a wheel, spinning at a constant angular velocity inside two or three actuated gimbals. Tilting the wheel's axis of rotation generates the gyroscopic torque. This system is widespread in spacecrafts reorientation [6], but less frequently exploited in robot locomotion, either wheeled [7] or legged [8]. The CMG presents interesting capabilities, but the presence of a pan-tilt unit to drive the gyroscope makes it impractical to mount it on a small, lightweight robot.

Flywheels represent an additional option for controlling the robot orientation. Changing the angular velocity of a rotating mass attached to the trunk generates a torque that can reorient the robot. This device has been first applied for spacecraft orientation [9], and later it has been only sporadically investigated in legged locomotion for controlling pitch orientation, both for bipeds [10], [11] and quadrupeds [12], [13]. Compared with tails, flywheels do not have position limits, and since their rotation axes pass through the CoM, its angular momentum results holonomic [14]. To get a fast response, it is necessary to have an abrupt change in the flywheels angular velocity (angular acceleration). Using a brake avoids the employment of a motor able to deliver higher torques [15], keeping the system compact: the motor slowly accelerates the wheel to a certain speed to store angular momentum and, when a reorientation is required, the break stops its spin. Since the effect of the break is unidirectional, a limitation of this approach is given by the fact that it is possible to generate a rotation of the base only in the opposite direction of the flywheel angular velocity making them unsuitable for applications where *continuous* controllability is required. On the other hand, direct-drive controlled flywheels enable to create accelerations in both directions, and to implement continuous control laws.
The benefits of this kind of OCS are multiple.

1. Flywheels can correct orientation errors during the flight (e.g. due to disturbances or tracking inaccuracies in the angular momentum achieved at the lift-off) in a continuous manner.
2. They enable to track a time-varying reference, e.g. to have the robot land with a desired angular velocity (possibly zero) and orientation.
3. Even in presence of contacts, they can enhance the landing phase or stabilize dynamic gaits (e.g. trot), by significantly reducing trunk oscillations.

4. The presence of these additional joints, whose only function is to control the orientation, gives the possibility to relieve the effort of the legs.

In more complex scenarios, like for a somersault, limbs and OCS can operate in parallel to achieve a rotation angle larger than the one achievable only with legs (e.g., due to torque limitation).

1.1. Proposed Approach and Contribution

In this work, we present a compact OCS based on two flywheels, mounted on the trunk of the lightweight quadruped Solo12 [16], see Fig. 1. The contributions of the paper are:

- the design of a novel OCS that enables to control the orientation of a legged robot during a jump in an effective way, while keeping the design simple. In particular, the axes of rotation of the flywheels are set to be incident, enabling *continuous* controllability in both the directions (roll and pitch) while keeping the device compact.
- simulations with the quadruped Solo12 that demonstrate the effectiveness of the proposed approach.

1.2. Outline

The remainder of this paper is organized as follow. In Section 2, the law of conservation of the total angular momentum is recalled. In Section 3, the design principles are presented together with the strategy for simultaneously control the robot roll and pitch orientations. Section 4 presents simulation in different scenarios that demonstrate the the capability of our OCS to reject disturbances and to track angular references when there is no contact with the ground, and damping of base oscillation after the touch-down. Conclusions and a possible evolution of the work ar reported in Section 5.

2. Background

The starting point for any OCS is the Euler's equation. For any mechanical system, the time derivative of the angular momentum $\boldsymbol{L}$ computed with the respect to a reference point O, fixed in an inertial frame, equals the sum of the moments $\boldsymbol{M}_i$ applied to the system with respect to the same reference point:

$$\dot{\boldsymbol{L}} = \sum_i \boldsymbol{M}_i \tag{1}$$

When the resultant of the external moments applied to the system is zero, the Euler's equation simplifies to:

$$\dot{\boldsymbol{L}} = 0 \quad \Rightarrow \quad \boldsymbol{L}(t) = const, \tag{2}$$

which is known as conservation of angular momentum. Referring to legged robots, this condition occurs when the system is not in contact with the ground or other objects, e.g., during a fall or the flight phase of a jump. In this case, it is possible to change the angular velocity of the base link changing the joint positions and velocities, as a result of the *nonholonomy* of the total angular momentum [17]: if the angular momentum of a certain body changes, the one of the others must change to maintain the total sum constant.

2.1. Preliminary Analysis

Most of quadruped robots are designed in such a way that the largest amount of the mass is located at the main body. As a consequence, the contribution of the moments due to the acceleration of other bodies (i.e. leg links) is moderate.
As an example, let consider the case of Solo12. Even if each limb accounts for about 13.4% of the total mass, changes of the total robot inertia come with the motion of only the upperleg (thigh) and the lowerleg (calf), since the displacement of distribution of the hip mass with the system CoM is approximately constant. In view of this, each limb accounts for only

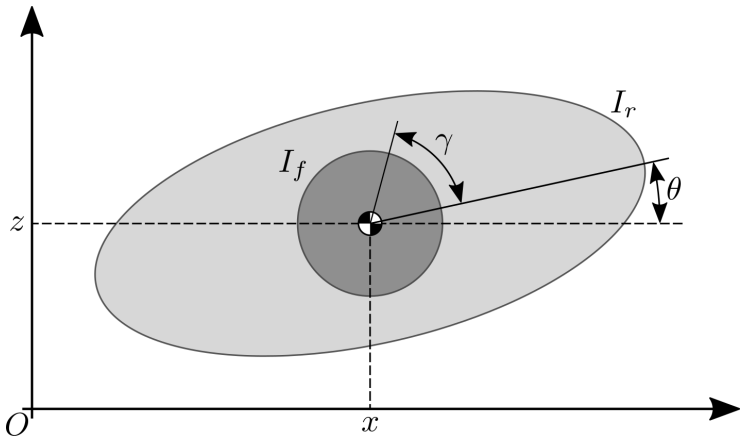

Figure 2. Schematic representation of the Elroy's Beanie model used for the preliminary analysis of the pitch motion.

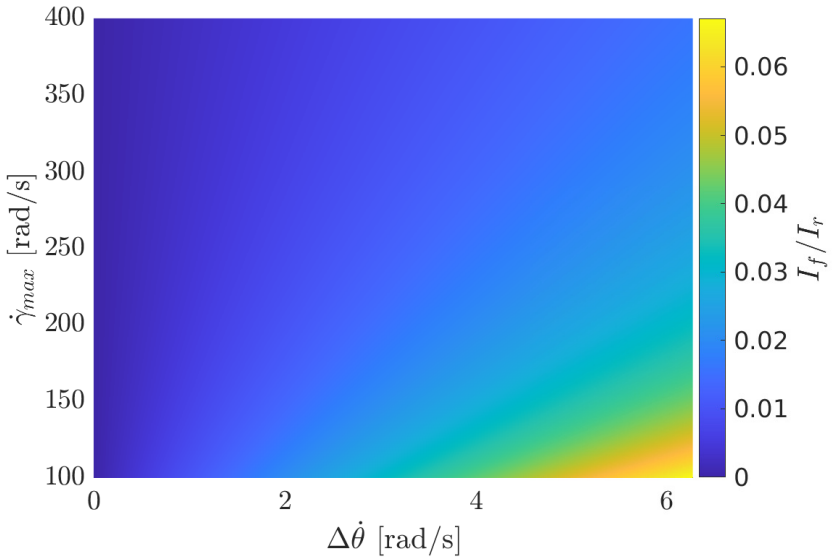

Figure 3. Minimum inertia of the OCS (normalized by the robot inertia) necessary to achieve a base velocity variation $\Delta\dot{\theta}$, given the actuation bound $\dot{\gamma}^{max}$.

7.5% of the total mass in varying the the total robot inertia. Flywheels can be used for alleviating the lack of control authority.

3. Orientation Control System

In this section, we present a procedure to select the inertia of the flywheels, and we show how to exploit them for simultaneously controlling the robot roll and pitch orientation.

3.1. Bounds on the Inertia

Investigation for the selection of the flywheels' inertia can be performed with the Elroy's Beanie model, depicted in Fig. 2. This consists of two rigid bodies connected through their CoM with a revolute joint. One of the bodies represents the robot in its nominal configuration. The other models the OCS, here represented by a single wheel for the sake of simplicity. The aim is to examine the rotational dynamics of the system as a whole. To simplify the analysis, in the following we will refer only to the effects on the pitch angle of the robot, keeping in mind that the same arguments apply also to the roll. Let us identify the moment of inertia of the robot in the nominal configuration as I_r and the

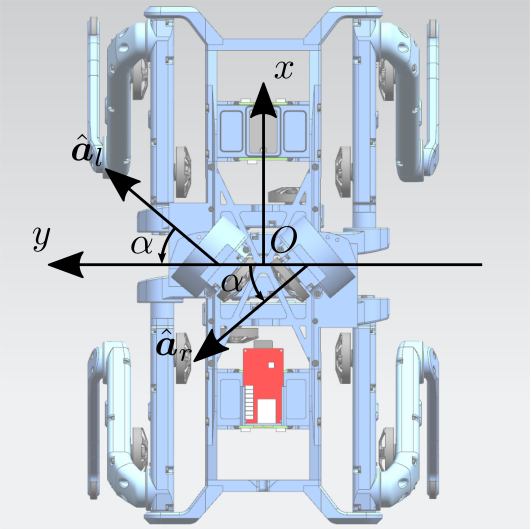

Figure 4. Representation of the flywheels rotation axes, seen from the top of the robot.

moment of inertia of the two flywheels as I_f, both referred to the system CoM. The angular momentum L of this system can be written as

$$L(t) = \Big(I_r + I_f\Big)\dot{\theta}(t) + I_f\dot{\gamma}(t) \tag{3}$$

where $\dot{\theta}$ and $\dot{\gamma}$ are respectively the robot pitch rate and the angular speed of the wheel. We want to drive the robot to a desired pitch rate $\dot{\theta}_{des}$ by acting on the wheel speed. Without loss of generality, we can assume the flywheel is stationary with the robot at the instant at which the reorientation maneuver starts ($\dot{\gamma}_0 = 0$), having a system angular momentum of $L_0 = \Big(I_r + I_f\Big)\dot{\theta}_0$. Under the condition of conservation of the angular momentum, this quantity is constant over time and it is possible to estimate the lower bound for I_f given a desired pitch rate and the maximum velocity of the flywheels $\dot{\gamma}_{max}$:

$$I_f \geq I_r \frac{\Delta\dot{\theta}}{\Delta\dot{\theta} + \dot{\gamma}_{max}}. \tag{4}$$

where $\Delta\dot{\theta} = \left|\dot{\theta}_0 - \dot{\theta}_{des}\right|$ is the base velocity variation. Fig. 3 reports the lower bound of I_f given the desired base velocity variation and the maximum velocity of the actuator.

3.2. Flywheels Axes of Rotation

The orientation of the axis of rotation of each flywheel influences their contribution to the total angular momentum. To meet the specification of controlling both the robot roll and pitch, the axes of rotation of the left and right wheel, identified in the base reference frame with the unit vectors $\hat{\boldsymbol{a}}_l$ and $\hat{\boldsymbol{a}}_r$, are set to be incident, laying on a plane parallel to the $xy-$plane of the base reference frame (see Fig. 4). To remove unnecessary complications, we designed two identical modules, to be mounted on the trunk of Solo12, symmetrically with the respect of the robot sagittal plane. We denote with $\alpha \leq \pi/2$ the non-negative incident angle between the wheels' axes of rotation and the robot lateral direction. The matrix

$$\boldsymbol{C} = \begin{bmatrix} \hat{\boldsymbol{a}}_l & \hat{\boldsymbol{a}}_r \end{bmatrix} = \begin{bmatrix} \sin(\alpha) & -\sin(\alpha) \\ \cos(\alpha) & \cos(\alpha) \\ 0 & 0 \end{bmatrix} \tag{5}$$

maps the flywheel moments into scalar torques $\boldsymbol{u} = \begin{bmatrix} \tau_{fl} & \tau_{fr} \end{bmatrix}^T$ about the flywheel axes $\hat{\boldsymbol{a}}_l$ and $\hat{\boldsymbol{a}}_r$ (expressed in the base frame). As long as $\boldsymbol{C}$ is full column rank, it is possible to control both roll and pitch angles. If $\alpha = 0$, the roll results to be uncontrollable through the

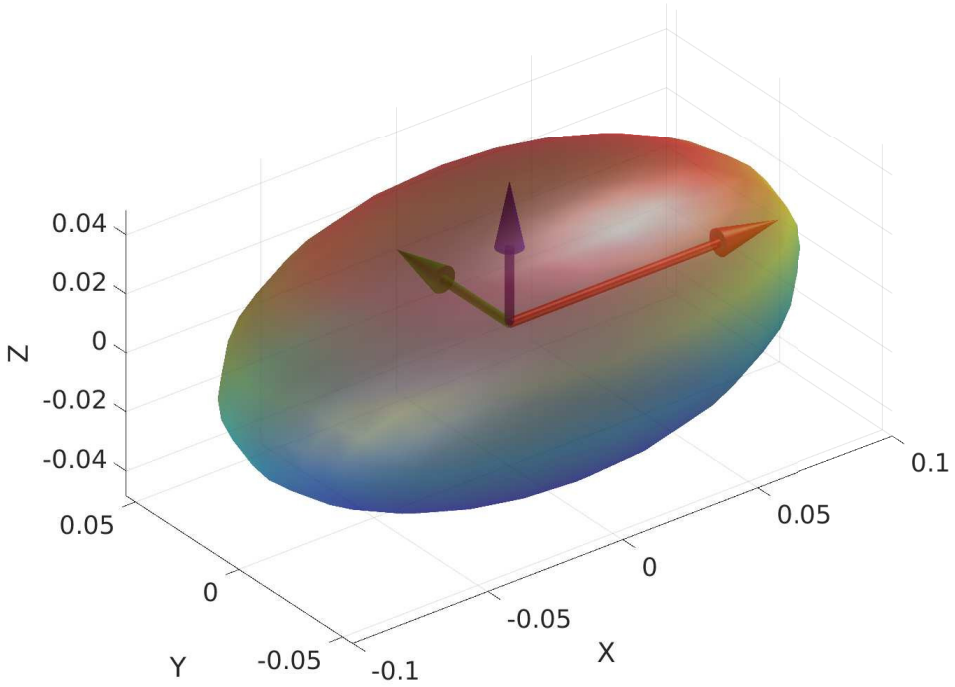

Figure 5. The inertia tensor can be seen as an ellipsoid. Its principal axes in the direction of the eigenvectors of the tensor and their length depends on the eigenvalues.

OCS; otherwise, if $\alpha = \pi/2$, the pitch is uncontrollable. The angle is selected considering the ratio of the eigenvalues along the x and y directions of the ellipsoid of the robot inertia(Fig. 5):

$$\alpha^* = \tan^{-1}\left(\frac{I_{r,xx}}{I_{r,yy}}\right).$$

In the case of Solo12, this angle is about $40°$. With these considerations, the angular momentum produced by the wheels, expressed in the robot base frame, is:

$$\begin{aligned} {}_b\boldsymbol{L}_f &= {}_b\boldsymbol{L}_{fl} + {}_b\boldsymbol{L}_{fr} \\ &= I_{f,zz}\,\boldsymbol{\omega}_{fl} + I_{f,zz}\,\boldsymbol{\omega}_{fr} \\ &= I_{f,zz}\begin{bmatrix} \left(\omega_{fl} - \omega_{fr}\right)\sin(\alpha) \\ \left(\omega_{fl} + \omega_{fr}\right)\cos(\alpha) \\ 0 \end{bmatrix} \end{aligned} \tag{6}$$

in which $\boldsymbol{\omega}_{fl} = \omega_{fl}\,\hat{\boldsymbol{a}}_l$ and $\boldsymbol{\omega}_{fr} = \omega_{fr}\,\hat{\boldsymbol{a}}_r$ are the angular velocity vectors of the two wheels, and ω_{fl} and ω_{fr} are the angular speeds provided to each flywheel by its actuation system. The latter equation shows that the difference of the two angular speeds impacts on roll rotations, while their difference can be used to adjust the pitch, see Fig. 6. Using the definition of $\boldsymbol{C}$, (6) rewrites as

$$\begin{aligned} {}_b\boldsymbol{L}_f &= I_{f,zz}\begin{bmatrix} \sin(\alpha) & -\sin(\alpha) \\ \cos(\alpha) & \cos(\alpha) \\ 0 & 0 \end{bmatrix}\begin{bmatrix} \omega_{fl} \\ \omega_{fr} \end{bmatrix} \\ &= I_{f,zz}\boldsymbol{C}\boldsymbol{\omega}_f. \end{aligned} \tag{7}$$

117

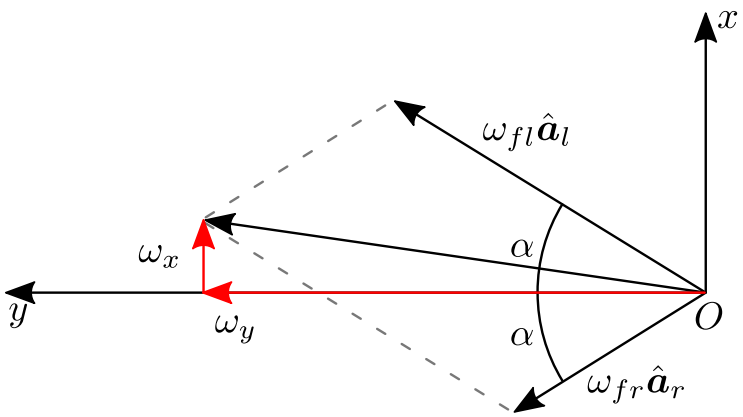

Figure 6. Having incident rotation axes, the OCS allows to control both the robot roll and pitch. Notice that the roll angle is influenced by the difference of the angular speeds of the flywheels, $\omega_x = \left(\omega_{fl} - \omega_{fr}\right) \sin(\alpha)$. On the contrary, the pitch angle depends on the sum of the angular speeds $\omega_y = \left(\omega_{fl} + \omega_{fr}\right) \cos(\alpha)$.

3.3. Inertia Selection

Once the desired inertia I_f is chosen, according to the 2D Elroy's Beanie model, it is used to realize the 3D OCS (Fig. 7). We decided to design the flywheels in the shape of hollow cylinders. This shape increases the inertia by locating the mass far away from the rotation axis. The inertia tensor expressed in its principal axes, $\boldsymbol{I}_f = \text{diag}\left\{I_{f,xx},\, I_{f,yy},\, I_{f,zz}\right\}$, depends on the cylinders inner and outer radii, r and R, its height h and the material density ρ:

$$\begin{aligned} I_{f,xx} = I_{f,yy} &= \frac{1}{12}\pi\rho h\left(3\left(R^4 - r^4\right) + h^2\left(R^2 - r^2\right)\right) \\ I_{f,zz} &= \frac{1}{2}\pi\rho h\left(R^4 - r^4\right) \end{aligned} \tag{8}$$

Notice that in the Elroy's Beanie model, there is a single body that models the complete OCS. The inertia introduced in the Elroy's Beanie model has to be split between the two flywheels: $I_{f,zz} = I_f / (2\cos(\alpha))$. The parameters R and h can be set to have a compact OCS and ρ depends on the chosen material, that is stainless steel in our case. The inner radius r can be adjusted to obtain the desired inertia. Spokes with negligible mass connect the wheel to the motor shaft. All the parameters are reported in Table 1, together with the selected inertia and mass of a single flywheel.

Table 1. Sizes and dynamic parameters of a single flywheel

Parameter	Value	Unit
r	$2.20 \cdot 10^{-2}$	m
R	$3.00 \cdot 10^{-2}$	m
h	$1.02 \cdot 10^{-2}$	m
ρ	$7.86 \cdot 10^{+3}$	kg/m^3
m	$1.02 \cdot 10^{-1}$	kg
I_{xx}, I_{yy}	$3.64 \cdot 10^{-5}$	$\text{kg} \cdot \text{m}^2$
I_{zz}	$7.11 \cdot 10^{-5}$	$\text{kg} \cdot \text{m}^2$

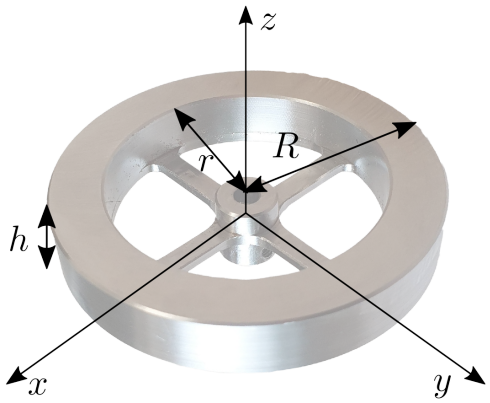

Figure 7. The final design of the flywheel, shown together with its inertia principal axes. Here, h is the wheel thickness, r is the inner radius of the wheel and R is the outer one.

3.4. Flywheels Control Law

To derive a control law based on the robot base orientation, we make use of (2), expressing all the contributions to the time derivative of total angular momentum with the respect to the base reference frame:

$$ {}_b\boldsymbol{I}_f \, {}_b\dot{\boldsymbol{\omega}}_f + {}_b\boldsymbol{I}_r \, {}_b\dot{\boldsymbol{\omega}}_r + {}_b\boldsymbol{\omega}_r \times ({}_b\boldsymbol{I}_r \, {}_b\boldsymbol{\omega}_r) = 0 $$

From this expression, we can define the moment on the base caused by the acceleration of the flywheels, that can be used as a feedback torque $\boldsymbol{\tau}_{fb}$:

$$ \begin{aligned} \boldsymbol{\tau}_{fb} &= \boldsymbol{I}_f \dot{\boldsymbol{\omega}}_f \\ &= -{}_b\boldsymbol{I}_r \dot{\boldsymbol{\omega}}_b - {}_b\boldsymbol{\omega}_r \times ({}_b\boldsymbol{I}_r \, {}_b\boldsymbol{\omega}_r) \end{aligned} $$

We can use the PD action $\boldsymbol{K}_p\boldsymbol{e} + \boldsymbol{K}_d\dot{\boldsymbol{e}}_r$, where $\boldsymbol{K}_p$ and $\boldsymbol{K}_d$ are diagonal and positive-definite gain matrices for the error in attitude and angular velocity. The orientation error $\boldsymbol{e} \in SO(3)$ needs the algebra of the special rotational group to be computed. To avoid singular configurations, we represent the orientation with quaternions. The derivative error can be computed using $\dot{\boldsymbol{e}} = {}_b\boldsymbol{\omega}_r^{\,des} - {}_b\boldsymbol{\omega}_r$, in which ${}_b\boldsymbol{\omega}_r^{\,des}$ and ${}_b\boldsymbol{\omega}_r$ are, respectively, the desired and actual angular velocity of the base:

$$ \boldsymbol{\tau}_{fb} = -{}_b\boldsymbol{I}_r \left(\boldsymbol{K}_p\boldsymbol{e} + \boldsymbol{K}_d\dot{\boldsymbol{e}} \right) - {}_b\boldsymbol{\omega}_r \times ({}_b\boldsymbol{I}_r \, {}_b\boldsymbol{\omega}_r). $$

Projecting the moment $\boldsymbol{\tau}_{fb}$ onto the flywheel axes with $\boldsymbol{C}^T$, we obtain the control action $\boldsymbol{u}$

$$ \boldsymbol{u} = \boldsymbol{C}^T\boldsymbol{\tau}_{fb}. \tag{9} $$

4. Results of Simulations

To validate our OCS, we present three simulations on different scenarios. We want to test the capability of the proposed approach to: reject a disturbance when the robot is in the flight phase of a jump, damp trunk oscillations after the touch-down, and work in parallel with the joints of the legs to achieve a highly dynamic motion. All the simulations are performed in Gazebo. The robot full dynamics is modeled with Pinocchio [18]. The references for the joints of the legs are computed off-line using Crocoddyl [19] and tracked with a PD joint controller. The OCS is commanded to track base orientation references using the control law introduced in Subsection 3.4.[1]

[1] The video with all the simulations is available at web link https://www.dropbox.com/scl/fo/wevvl0zvfp8gofie6x7rw/h?dl=0&rlkey=pap76cr813a0skrvrxl7qgrb9.

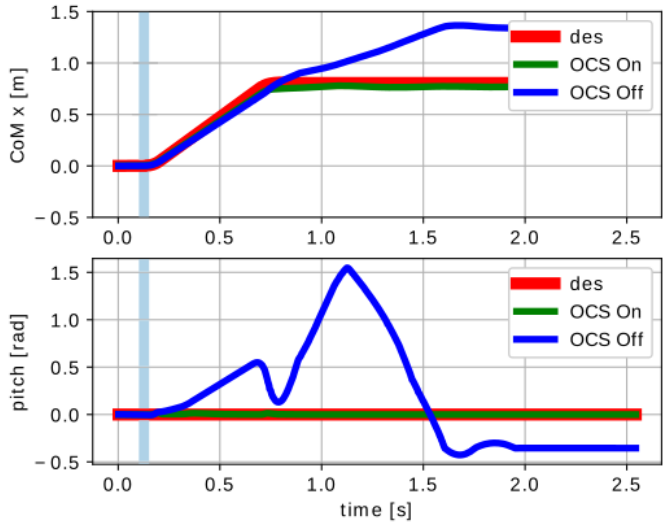

Figure 8. First Test: simulation results showing the CoM$_x$ and pitch trajectory vs. time plots. A disturbance moment τ_{dist} on the trunk can be compensated only if the OCS is enabled. If it is disabled, the robot is unable to restore a safe configuration after the touch-down and eventually falls. The light blue area represents the interval of time in which the disturbance is applied.

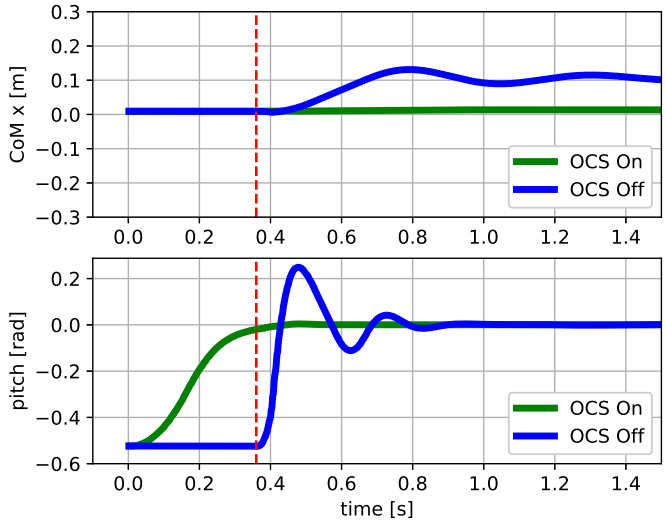

Figure 9. Second Test: simulation results showing the CoM$_x$ and pitch trajectory vs. time plots. The OCS drives the robot orientation during a fall to be horizontal. This allows to damp for damping the base oscillations after the touch-down (vertical dashed line), even without implementing a landing strategy

The necessity of having an OCS is revealed with the first test: disturbance that occurs when the robot has no contact with the ground. During the flight phase of a forward jump, 0.1 s after the lift-off, an external disturbance moment is applied to the robot base, deflecting the robot orientation: this disturbance is set to $\tau_{dist} = \begin{bmatrix} 0.2 & 0.8 & 0.0 \end{bmatrix}^T \mathrm{N \cdot m}$ and applied for 0.05 s. If the flywheels are not used, Solo12 falls after the touch-down. Instead, using the flywheels it is possible to drive the robot to a safe configuration after the landing (Fig. 8), without need to implement of a specific landing strategy, as the one in [20].

In the second test, we demonstrate the ability of the OCS to reorient the base. We let the robot fall from a height of 1 m with an initial pitch orientation of 30° and zero base angular velocity. If we do not actuate the flywheels, the robot touches the ground with the same initial orientation and the trunk oscillates. If the OCS is enabled, it drives the robot base to be horizontal when it is still in the air and the oscillations after the touch-down are drastically reduced, both in the pitch angle and forward direction (Fig. 9).

Finally, we demonstrate how flywheels can alleviate the effort of the leg joints to achieve a highly dynamic motion: a back-flip. For this, we target a space application carrying out a simulation with Moon gravity (1.62 m/s^2). In this way, it is possible to obtain high jumps with a long flight phase, without having to select more powerful actuators. The leg joint trajectory computed off-line describes a purely vertical jump of 1 m, having a flight phase that lasts 2 s. Right after the lift-off, the flywheels start the reorientation task of performing a back-flip, that is a spin of 360° on the pitch. For this maneuver, the value of the incident angle α is set to 0° since no roll rotation is required. Our hardware design allows the manual change of this value before performing the task. This simulation demonstrates that the OCS alleviate the effort to be applied on the legs: indeed, that it would not have been possible to do a back-flip without the flywheels because the legs are used only to achieve the linear motion.

5. Conclusions

In this work, we have presented the design of a novel OCS, composed of two flywheels, that enables to control the trunk of a legged robot platform, increasing the accuracy of aerial maneuvers during the under-actuated phases (i.e. flight phase) as well as enhancing stability when in contact by damping oscillations. The novelty of the design, that involves the flywheels to be attached with incident rotational axes on the trunk, allows to control the orientation in both the roll and pitch directions while keeping the device compact. Their effect is optimized considering the inertial property of the mechanical structure. Several simulations are reported with the quadruped Solo12 that demonstrate the effectiveness of the proposed approach to: reject disturbances during the flight phase, stabilize the platform after the touch-down even in absence of a specific landing strategy and achieve a fast reorientation maneuver (a back-flip) in a reduced gravity environment.

In future works, we plan to demonstrate our concept performing experiment with the real platform. The control strategy for defining the base desired angular velocity can be improved using Nonlinear Model Predictive Control (NMPC), that takes into consideration the future samples of the orientation reference. We expect this feature will allows the stabilization of the yaw to a desired value, that if it is not locally controllable, enhancing the non-holonomy property of the angular momentum, i.e. doing a preliminary roll and pitch maneuver. A control strategy that may lead to the same result is dynamic feedback linearization, widely used for flight with quadricopters.

Author Contributions: Conceptualization, F.R. and M.F.; software, F.R., A.C. and M.F.; validation, F.R., A.C. and M.F.; formal analysis, F.R., A.C. and M.F.; investigation, F.R. and A.C.; resources, C.S.; data curation, F.R., A.C. and M.F.; writing—original draft preparation, F.R.; writing—review and editing, F.R., A.C., A.D.P., C.S. and M.F.; visualization, F.R. and A.C.; supervision, A.D.P. and M.F; project administration, F.R. and M.F.; funding acquisition, M.F., C.S. All authors have read and agreed to the published version of the manuscript.

Funding: The publication was created with the co-financing of the European Union FSE-REACT-EU, PON Research and Innovation 2014-2020 DM1062 / 2021.

Institutional Review Board Statement: Not applicable.

Informed Consent Statement: Not applicable.

Data Availability Statement: Not applicable.

Acknowledgments: All the authors want to thank Dr. Roy Featherstone for interesting tips that started this work.

Conflicts of Interest: The authors declare no conflict of interest.

Abbreviations

The following abbreviations are used in this manuscript:

CoM	Center Of Mass
OCS	Orientation Control System
CMG	Control Moment Gyroscope
NMPC	Nonlinear Model Predictive Control

References

1. Kane, T.; Scher, M. A dynamical explanation of the falling cat phenomenon. *International journal of solids and structures* **1969**, *5*, 663–670.
2. Chu, X.; Lo, C.H.D.; Ma, C.; Au, K.W.S. Null-Space-Avoidance-Based Orientation Control Framework for Underactuated, Tail-Inspired Robotic Systems in Flight Phase. *IEEE Robotics and Automation Letters* **2019**, *4*, 3916–3923.
3. Wenger, G.; De, A.; Koditschek, D.E. Frontal plane stabilization and hopping with a 2DOF tail. In Proceedings of the 2016 IEEE/RSJ International Conference on Intelligent Robots and Systems (IROS). IEEE, 2016, pp. 567–573.
4. Johnson, A.M.; Libby, T.; Chang-Siu, E.; Tomizuka, M.; Full, R.J.; Koditschek, D.E. Tail assisted dynamic self righting. In *Adaptive mobile robotics*; World Scientific, 2012; pp. 611–620.
5. Hoffman, E.M.; Paolillo, A. Exploiting visual servoing and centroidal momentum for whole-body motion control of humanoid robots in absence of contacts and gravity. In Proceedings of the 2021 IEEE International Conference on Robotics and Automation (ICRA). IEEE, 2021, pp. 2979–2985.
6. Yoon, H.; Tsiotras, P. Spacecraft adaptive attitude and power tracking with variable speed control moment gyroscopes. *Journal of Guidance, Control, and Dynamics* **2002**, *25*, 1081–1090.
7. Brown, H.B.; Xu, Y. A single-wheel, gyroscopically stabilized robot. In Proceedings of the Proceedings of ieee international conference on robotics and automation. IEEE, 1996, Vol. 4, pp. 3658–3663.
8. Mikhalkov, N.; Prutskiy, A.; Sechenev, S.; Kazakov, D.; Simulin, A.; Sokolov, D.; Ryadchikov, I. Gyrubot: nonanthropomorphic stabilization for a biped. In Proceedings of the 2021 IEEE International Conference on Robotics and Automation (ICRA). IEEE, 2021, pp. 4976–4982.
9. Oland, E.; Schlanbusch, R. Reaction wheel design for cubesats. In Proceedings of the 2009 4th International Conference on Recent Advances in Space Technologies. IEEE, 2009, pp. 778–783.
10. Brown, T.L.; Schmiedeler, J.P. Reaction Wheel Actuation for Improving Planar Biped Walking Efficiency. *IEEE Transactions on Robotics* **2016**, *32*, 1290–1297. https://doi.org/10.1109/TRO.2016.2593484.
11. Xiong, X.; Ames, A.D. Sequential motion planning for bipedal somersault via flywheel slip and momentum transmission with task space control. In Proceedings of the 2020 IEEE/RSJ International Conference on Intelligent Robots and Systems (IROS). IEEE, 2020, pp. 3510–3517.
12. Kolvenbach, H.; Hampp, E.; Barton, P.; Zenkl, R.; Hutter, M. Towards jumping locomotion for quadruped robots on the moon. In Proceedings of the 2019 IEEE/RSJ International Conference on Intelligent Robots and Systems (IROS). IEEE, 2019, pp. 5459–5466.
13. Vasilopoulos, V.; Machairas, K.; Papadopoulos, E. Quadruped pronking on compliant terrains using a reaction wheel. In Proceedings of the 2016 IEEE International Conference on Robotics and Automation (ICRA). IEEE, 2016, pp. 3590–3595.
14. Machairas, K.; Papadopoulos, E. On quadruped attitude dynamics and control using reaction wheels and tails. In Proceedings of the 2015 European Control Conference (ECC). IEEE, 2015, pp. 753–758.
15. Gajamohan, M.; Merz, M.; Thommen, I.; D'Andrea, R. The cubli: A cube that can jump up and balance. In Proceedings of the 2012 IEEE/RSJ International Conference on Intelligent Robots and Systems. IEEE, 2012, pp. 3722–3727.
16. Grimminger, F.; Meduri, A.; Khadiv, M.; Viereck, J.; Wüthrich, M.; Naveau, M.; Berenz, V.; Heim, S.; Widmaier, F.; Flayols, T.; et al. An open torque-controlled modular robot architecture for legged locomotion research. *IEEE Robotics and Automation Letters* **2020**, *5*, 3650–3657.
17. Wieber, P.B.; Tedrake, R.; Kuindersma, S., Modeling and Control of Legged Systems. In *Springer Handbook of Robotics, 2nd Ed*; Siciliano, B.; Khatib, O., Eds.; Springer, 2016.
18. Carpentier, J.; Saurel, G.; Buondonno, G.; Mirabel, J.; Lamiraux, F.; Stasse, O.; Mansard, N. The Pinocchio C++ library – A fast and flexible implementation of rigid body dynamics algorithms and their analytical derivatives. In Proceedings of the IEEE International Symposium on System Integrations (SII), 2019.
19. Mastalli, C.; Budhiraja, R.; Merkt, W.; Saurel, G.; Hammoud, B.; Naveau, M.; Carpentier, J.; Righetti, L.; Vijayakumar, S.; Mansard, N. Crocoddyl: An efficient and versatile framework for multi-contact optimal control. In Proceedings of the 2020 IEEE International Conference on Robotics and Automation (ICRA). IEEE, 2020, pp. 2536–2542.
20. Jeon, S.H.; Kim, S.; Kim, D. Real-time Optimal Landing Control of the MIT Mini Cheetah. *arXiv preprint arXiv:2110.02799* **2021**.